Inorganic Chemistry

Article

pubs.acs.org/IC

Series of 2D Heterometallic Coordination Polymers Based on Ruthenium(III) Oxalate Building Units: Synthesis, Structure, and Catalytic and Magnetic Properties

Alla Dikhtiarenko,[†] Sergei A. Khainakov,[†] Imanol de Pedro,[‡] Jesús A. Blanco,[§] José R. García,*[,†] and José Gimeno[†]

[†]Departamento de Química Orgánica e Inorgánica, Universidad de Oviedo—CINN, 33006 Oviedo, Spain

[‡]CITIMAC, Facultad de Ciencias, Universidad de Cantabria, Avenida de los Castros 39005 Santander, Spain

[§]Departamento de Física, Universidad de Oviedo—CINN, 33007 Oviedo, Spain

Supporting Information

ABSTRACT: A series of 2D ruthenium-based coordination polymers with hcb-hexagonal topology, $\{[K(18\text{-crown-}6)]_3[M^{II}_3(H_2O)_4\{Ru(ox)_3\}_3]\}_n$ (M^{II} = Mn (**1**), Fe (**2**), Co (**3**), Cu (**4**), Zn (**5**)), has been synthesized through self-assembly reaction. All compounds are isostructural frameworks that crystallize in the monoclinic space group *C*2/*c*. The crystal packing consists of a 2D honeycomb-like anionic mixed-metal framework intercalated by $[K(18\text{-crown-}6)]^+$ cationic template. Dehydration processes take place in the range 40−200 °C exhibiting two phase transitions. However, the spontaneous rehydration occurs at room temperature. Both hydrated and dehydrated compounds were tested as Lewis acids heterogeneous catalysts in the acetalyzation of benzaldehyde achieving high yields with the possibility to be recovered and reused. All the investigated materials do not show any long-range magnetic ordering down to 2 K. However, the Fe-based compound **2** presents a magnetic irreversibility in the ZFC-FC magnetization data below 5 K, which suggest a spin-glass-like behavior, characterized also by short-range ferromagnetic correlations. The coercive field increases as the temperature is lowered below 5 K, reaching a value of 1 kOe at 2 K. Alternating current measurements obtained at different frequencies confirm the freezing process that shows weak frequency dependence, being characteristic of a system exhibiting competing magnetic interactions.

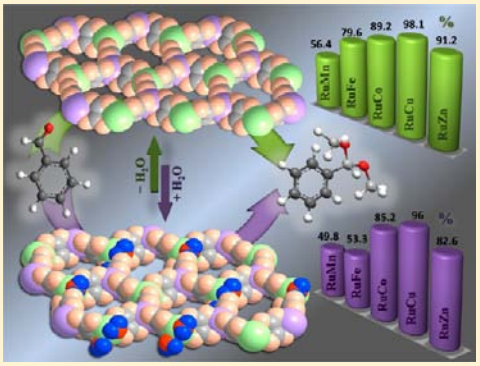

INTRODUCTION

During the past decade, synthesis and studies of coordination polymers (CPs) have received considerable attention[1] because of their widely functional properties including catalysis,[2] ion-exchange,[3] gas storage and separation,[4] luminescence,[5] and magnetic behaviors.[6] Among them, heterometallic coordination polymers (HCPs) formed by building blocks with different chemical nature are particularly interesting due to their diverse functionality. The building blocks used in the synthesis of heterometallic polymers are known as metalloligands. Contrary to organic ligands, metalloligands act as bridging ligands incorporating several advantages: multicoordination sites, flexible geometric control, and the ability to assemble a discrete unit into a polymeric frame giving rise to polymeric heterometallic frameworks with appealing structural and/or physicochemical properties.[1a]

One of the most successful strategies for preparing functional heterometallic coordination polymers is the self-assembly of polyhedral coordination-donor building blocks with a second metal center/metalloligand unit which provides additional coordination sites. Most of the reported investigations have been devoted to HCPs containing d−f[7] or d−d[8] metal centers. The d−d polynuclear compounds have been found to exhibit interesting magnetic properties varying from paramagnetic to ferromagnetic or antiferromagnetic behaviors. The most striking examples belong to the family of oxalate (ox) bridged mixed-metal coordination polymers of general formula $A\text{-}[M^{II}M^{III}(ox)_3]_n$ [M^{II} = Mn, Fe, Co, Ni, Cu, Zn; M^{III} = Cr, Fe, V, Mn; A = XR_4 (X = N, P, As; R = *n*-C_2H_5, *n*-C_4H_9, *n*-C_3H_7, *n*-C_5H_{11}, C_6H_5, $C_6H_5CH_2$, $[(C_6H_5)_3PNP(C_6H_5)_3)]_{0.25}$ or $[K(18\text{-crown-}6)]^+$ cationic metal-complex)][9,10] in which the oxalate dianion acts as a bridging ligand forming extended networks of either 2D or 3D dimensionalities.[11] In these compounds, the extended anionic bimetallic network $[M^{II}M^{III}(ox)_3]_n$ combined with a molecular bulky cation (A) which acts as a sort of template controlling the type of the resulting structure. In particular, the 2D network series displays honeycomb-like layer topology built by octahedral M^{II} and M^{III} geometries and tris-chelate oxalate sites in which the oxalate ligand is shown to be a useful tool in the spatial arrangement of spin-carrying metal ions.[12] These layered structures may provide structural and chemical versatility as can be shown by magnetic properties which are tuned by changing the electronic nature of interlayer

Received: December 11, 2012
Published: March 11, 2013

   dx.doi.org/10.1021/ic302725v | *Inorg. Chem.* 2013, 52, 3933−3941

Table 1. Crystallographic Data for Compounds 1−5

	1	2	3	4	5
empirical formula	$C_{54}H_{80}K_3Mn_3O_{58}Ru_3$	$C_{54}Fe_3H_{80}K_3O_{58}Ru_3$	$C_{54}Co_3H_{80}K_3O_{58}Ru_3$	$C_{54}Cu_3H_{80}K_3O_{58}Ru_3$	$C_{54}H_{80}K_3O_{58}Ru_3Zn_3$
fw	2242.51	2244.33	2254.48	2268.34	2273.86
cryst syst	monoclinic	monoclinic	monoclinic	monoclinic	monoclinic
space group	*C*2/*c*	*C*2/*c*	*C*2/*c*	*C*2/*c*	*C*2/*c*
a, Å	26.896(4)	26.620(3)	26.539(9)	26.547(5)	26.593(7)
b, Å	19.840(3)	19.908(3)	20.025(7)	19.279(4)	19.230(7)
c, Å	18.129(2)	18.009(2)	18.036(6)	17.995(3)	18.192(5)
β, deg	115.8(6)	115.3(5)	115.3(1)	113.8(1)	114.1(1)
V, Å^3	8710(2)	8625(2)	8664(5)	8425(3)	8495(4)
Z	4	4	4	4	4
ρ_{calcd}, g cm^{-3}	1.710	1.728	1.728	1.788	1.778
T, K	298	298	298	298	298
R_p, R_{wp}	4.56, 5.97	3.25, 4.30	2.66, 3.65	4.12, 5.25	6.32, 8.03
R_B	7.65	10.2	8.81	8.12	7.86

and network components. On the basis of this particular behavior, this family of compounds may be taken as illustrative examples to attain desirable functional properties. In spite of the versatile coordination chemistry, catalytic properties, and magnetic behavior of ruthenium complexes,[13] to date only two examples of oxalate bridged HCPs of general formula $[M^{III}Cp_2][M^{II}Ru^{III}(ox)_3]_n$ (M^{III} = Co, Fe; M^{II} = Mn, Fe, Co, Cu, Zn; Cp = pantamethylcyclopentadienyl) and $[NBu_4]$-$[M^{II}Ru^{III}(ox)_3]_n$ (M^{II} = Mn, Fe, Cu) containing $[Ru(ox)_3]^{3-}$ building units have been reported.[14] Therefore, inspired by potential magnetic properties of $[M^{II}Ru^{III}(ox)_3]_n$ mixed-metal frameworks and attractive catalytic features of ruthenium complexes,[15] our investigation has been focused on the rational structural and functional design of $Ru(ox)_3$-based heterometallic coordination polymers.

Herein, we report the synthesis and structural characterization of the 2D series of $\{[(K\text{-}18\text{-}crown\text{-}6)_3][M_3^{II}(H_2O)_4(Ru(ox)_3)_3]\}_n$ (M^{II} = Fe, Co, Cu, Mn, Zn; ox = C_2O_4) heterometallic coordination polymers resulting from self-assembling reaction of the $[Ru(ox)_3]^{3-}$ salt, acting as metalloligand, with corresponding transition metal ions. Also, their thermal, catalytic, and magnetic behaviors have been discussed. The dehydrated compounds $\{[(K\text{-}18\text{-}crown\text{-}6)][M^{II}(Ru(ox)_3]\}_n$ (M^{II} = Fe, Co, Cu, Mn, Zn) have been isolated and characterized exhibiting reversible rehydration process and high catalytic activity in Lewis acid promoted reaction.

EXPERIMENTAL SECTION

Materials and Methods. All reagents and solvents used were of commercially available grade and were used without any previous purification. $K_3[Ru(ox)_3]\cdot 4.5H_2O$ was prepared according to a previously described method.[16]

The IR spectra were recorded on a Bruker Tensor-27 spectrophotometer as KBr pellets in the 4000−400 cm^{-1} region. Microanalyses (C, H, N) were completed by the use of a Perkin-Elmer model 2400B elemental analyzer. The microcrystalline texture of samples and metal contents were confirmed by using a JEOL JSM-6100 scanning microscopy (SEM) coupled with an INCA Energy-200 dispersive X-ray microanalysis system (EDX), and a PentaFET ultrathin window detector. Mettler-Toledo TGA/SDTA851 and DSC822 were used for the thermal analyses in nitrogen (or air) dynamic atmosphere (50 mL/min) at a heating rate of 10 °C/min (approximately 10 mg of powder sample was thermally treated, and blank runs were performed). A Pfeiffer Vacuum TermoStar GSD301T mass spectrometer was used to determine the evacuated vapors. The masses 18 (H_2O) and 44 (CO_2) were tested by using a detector C-SEM, operating at 1200 V, with a time constant of 1 s.

Magnetic susceptibility measurements were performed in PPMS (QD-PPMS) and SQUID (QD-PMPMS-5T) magnetometers in the temperature range 2−250 K. For measurements of the magnetization in a zero-field cooled (ZFC) state, the sample was cooled from the paramagnetic state in a zero applied field, and the magnetization was measured while warming the sample. The magnetization data in the field cooled (FC) state were collected while cooling the sample. Several magnetization versus field ($M(H)$) isotherms in fields up to 85 kOe were measured at different temperatures, cooling the sample every time from the paramagnetic state to the temperature of the measurement. Alternating curent magnetic susceptibility measurements were made using the SQUID device, with an alternating excitation field (h) of 3 Oe. Data were recorded from 2 to 10 K as a function of frequency, between 10 and 10^3 Hz, in the absence of a dc applied field.

Synthesis of $\{[K(18\text{-}crown\text{-}6)]_3[M^{II}_3(H_2O)_4\{Ru(ox)_3\}_3]\}_n$ (M^{II} = Mn (1), Fe (2), Co (3), Cu (4), Zn (5)). The synthesis process was performed in accordance with a previously published procedure[10a,b] for the $\{[(K\text{-}18\text{-}crown\text{-}6)_3][M_3^{II}(H_2O)_4(M^{III}(ox)_3)_3]\}_n$ (M^{III} = Cr, Fe; M^{II} = Mn, Fe, Ni, Co, Cu; ox = C_2O_4) series of compounds introducing $[Ru(ox)_3]^{3-}$ moiety instead of $[Cr(ox)_3]^{3-}$ or $[Fe(ox)_3]^{3-}$. In a typical synthesis, 124 mg (0.25 mmol) of $K_3[Ru(ox)_3]\cdot 4.5H_2O$ and 198 mg (0.75 mmol) of 18-crown-6 ether were dissolved in 10 mL of methanol, and 0.25 mmol of the transition metal salt ($MnCl_2\cdot 4H_2O$, 50 mg; $FeCl_2\cdot 4H_2O$, 49 mg; $CoCl_2\cdot 6H_2O$, 54 mg; $CuCl_2$, 34 mg; $ZnCl_2$, 34 mg) dissolved in 5 mL of methanol was added dropwise, immediately a precipitates appeared, and the mixture was stirred for 30 min. The methanolic solutions were filtered in vacuum, and the precipitates were washed with methanol and air-dried. Yellow precipitate of **1** yields 77%. Anal. for $C_{54}H_{80}K_3Mn_3O_{58}Ru_3$ (**1**): C, 28.92%; H, 3.57%. Found: C, 28.91%; H, 3.54%. Green precipitate of **2** yields 79%. Anal. for $C_{54}Fe_3H_{80}K_3O_{58}Ru_3$ (**2**): C, 28.89%; H, 3.56%. Found: C, 28.93%; H, 3.78%. Brown precipitate of **3** yields 74%. Anal. for $C_{54}Co_3H_{80}K_3O_{58}Ru_3$ (**3**): C, 28.13%; H, 3.47%. Found: C, 27.53%; H, 3.61%. Orange precipitate of **4** yields 81%. Anal. for $C_{54}Cu_3H_{80}K_3O_{58}Ru_3$ (**4**): C, 27.99%; H, 3.47%. Found: C, 25.38%; H, 3.72%. Yellow precipitate of **5** yields 70%. Anal. for $C_{54}H_{80}K_3O_{58}Ru_3Zn_3$ (**5**): C, 27.93%; H, 3.45%. Found: C, 26.91%; H, 3.62%.

X-ray Diffraction Characterization. Powder X-ray diffraction patterns were recorded on X'pert Philips diffractometer with Cu K*α* radiation. The samples were gently ground in an agate mortar. All data were collected at room temperature over the angular 2*θ* range 5−142° with a step of 0.013° and a counting time of 0.424 s/channel. The initial structure model was constructed from unit cell parameters and fractional atomic coordinates taken from previous reported analogous Cr-based compound.[10a,b] Rietveld refinement was performed in the range 2*θ* = 7−50° using Reflex module of Materials Studio,[17] applying Motion Group sets. As the rigid groups of atoms have been composed, there are Ru, M^{II}, K atoms, 18-crown-6, and oxalate ligand fragments.

dx.doi.org/10.1021/ic302725v | Inorg. Chem. 2013, 52, 3933−3941

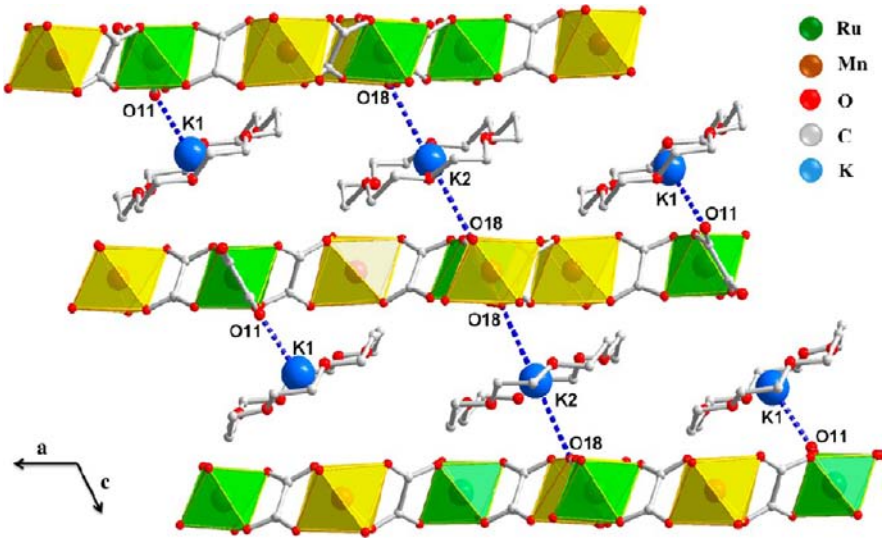

Figure 1. Perspective view along *b*-axis of heterometallic 2D layers and intercalated between them K(18-crown-6)$^+$ cations.

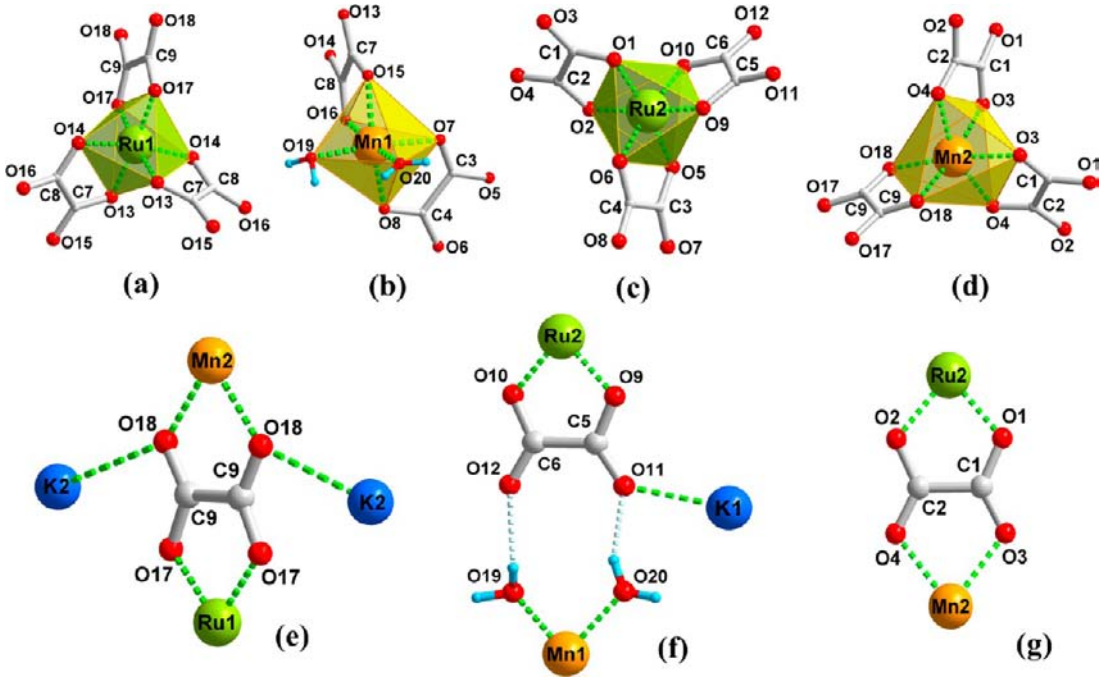

Figure 2. Coordination environments of Ru^{III} (a, c), Mn^{II} (b, d), and coordination modes of the oxalate ligand $\mu_4 = (\eta_2: \eta_1: \eta_2: \eta_1)$ (e), $\mu = (\eta_2: \eta_1)$ (f), and $\mu = (\eta_2: \eta_2)$ (g).

First, the zero offset, the scale factor, background terms, profile parameters, and the unit cell were refined. The profiles have been modeled as a pseudo-Voigt function. After that the atomic positions and global isotropic parameter were refined. In the final refinement the water molecules have been placed geometrically and fixed in this position. The unit cell parameters and the final values of figures of merit are listed in Table 1.

Powder X-ray thermodiffraction studies were performed in air with the sample placed in an Anton Paar XRK 900 reactor chamber on a Bruker D8 Advance diffractometer with DAVINCI design, using Cu Kα radiation, equipped with LynxEye detector. Each powder pattern was recorded in the 4−110° range of 2θ at intervals of 25 °C up to 195 °C and cooling down to 25 °C with a step of 0.015° and a counting time of 0.424 s/channel. The temperature ramp between two consecutive temperatures was 10 °C/min. The PXRD data acquisition and analysis in this work were carried out using Bruker AXS DIFFRAC.EVA software. The dehydrated **1a** and dehydrated **1b** compounds was indexed using DICVOL06 program.[18]

Catalytic Procedure of Benzaldehyde Acetalyzation with Trimethylorthoformate (TMOF). Under nitrogen atmosphere a benzaldehyde substrate (0.05 mL, 0.5 mmol) and TMOF (0.5 mL, 5 mmol) were added to a suspension of the corresponding catalyst (1 mol %) in 3 mL of tetrachloromethane used as a solvent. The reaction mixture was stirred in a 25 mL Schlenk tube at 70 °C in oil bath. The course of the reaction was monitored by regular sampling and analysis by GC-FID. After 24 h, the catalyst was isolated by centrifugation, washed, and reused on subsequent runs.

RESULTS AND DISCUSSION

The family of coordination polymers **1**−**5** has been isolated as microcrystalline powders with plate-like habits, as is shown from the micrograph analysis (Supporting Information, Figure

dx.doi.org/10.1021/ic302725v | Inorg. Chem. 2013, 52, 3933−3941

S1). Rietveld refinement shows the isostructurality of our synthesized materials between them and with the Cr- and Fe-based analogous series of compounds ($\{[K(18\text{-crown-}6)]_3[M^{II}_3(H_2O)_4\{M^{III}(ox)_3\}_3]\}_n$, where M^{III} = Cr, Fe; M^{II} = Mn, Fe, Ni, Co, and Cu) which was reported previously[10a,b] (see Figure S2). The layered heterometallic polymers with the general formula $\{[K(18\text{-crown-}6)]_3[M^{II}_3(H_2O)_4\{Ru(ox)_3\}_3]\}_n$, where M^{II} = Mn(**1**), Fe(**2**), Co(**3**), Cu(**4**), and Zn(**5**), crystallize in monoclinic space group *C*2/*c*. Details of crystallographic data are summarized in Table 1. The crystal cell parameters are slightly changed as function of M^{II} transition ion incorporated in coordination network. The remarkable aspect of these structures is the packing arrangement where the positive potassium complex $[K(18\text{-crown-}6)]^+$ is intercalated between the negative 2D sheets (see Figure 1). Herein, only the structure of compound **1** is described in detail. The asymmetric unit of **1** contains three pairs of crystallographically independent metal centers (Mn1 and Mn2, Ru1 and Ru2, K1 and K2): (i) Ru1 and Ru2 are six coordinated, in a octahedral geometry, by oxygen atoms from the oxalate ligands (Figure 2a,c); (ii) the six-coordinated Mn1 exhibits octahedral coordination environment with six oxygen atoms, four of them belonging to oxalate anion and other two from coordinated water molecules (Figure 2b); (iii) Mn2 is bonded to six oxygen atoms coming from these oxalate ligands in octahedral coordination environment; (iv) two crystallographically nonequivelent K1 and K2 ions incorporated in crown ring form a planar coordination environment with six oxygen atoms of ether; additionally, K1 coordinates to one oxygen atom of terminal oxalate ligand, and K2 is involved in strong electrostatic interaction with two oxygen atoms of two different oxalate ligands which belong to two adjacent layers (above and below), contributing to effective 3D packing (Figure 1). In this structure, the oxalate ligand exhibits three kinds of coordination modes (Figure 2e–g): mode e, oxalate exhibits μ_4-(η_2: η_1: η_2: η_1)-bridging mode where two oxygen atoms (O18) coordinate two K2 and chelate one Mn2, and the other two chelate the Ru1; mode f, the terminal oxalate ligand is coordinate to one K1 and chelate Ru2 in μ-(η_1: η_2)-bridging mode; mode g, oxalate ligand chelates Ru2 and Mn2 exhibiting μ-(η_2: η_2)-bridging mode. The oxalate dianion, which behaves as a μ-(η_2: η_2) bridge, connects one by one [Ru1O_6], [Mn1O_6], [Ru2O_6], and [Mn2O_6] polyhedra (primary building units) to form a motif (secondary building unit) (Figure 3a) running along *a*-direction, resulting in zigzag-like 1D chains (Figure 3b). These chains are further extended along *b*-axis by μ_4-(η_2: η_1: η_2: η_1) oxalate, which bridges [Mn2O_6] and [Ru1O_6] polyhedra, to result in a 2D honeycombed layer structure which consists of a large 14-member ring based on three 6-member rings. Inside of large rings, [Ru2O_6] and [Mn1O_6] polyhedra are hold together by hydrogen bonds coming from μ-(η_1: η_2) oxalate ligand chelated to Ru2 and coordinated water molecules to Mn1; these hydrogen bonds define three smaller 6-membered rings. That is, two of them are regular with dimensions *ca.* 8.9 Å × 9.5 Å and one is elongated with dimensions *ca.* 6.8 Å × 11.4 Å (Figure S3). From the topological point of view, the metal centers can be reduced to three connected nodes and the oxalate ligands can be considered as ditopic linker. Therefore, the 2D layer is represented as 2D heterometallic uninodal three-connected net of hcb hexagonal plane network type (Figure S4) with Schläfli symbol 6^3, which agrees with TOPOS analysis.[19]

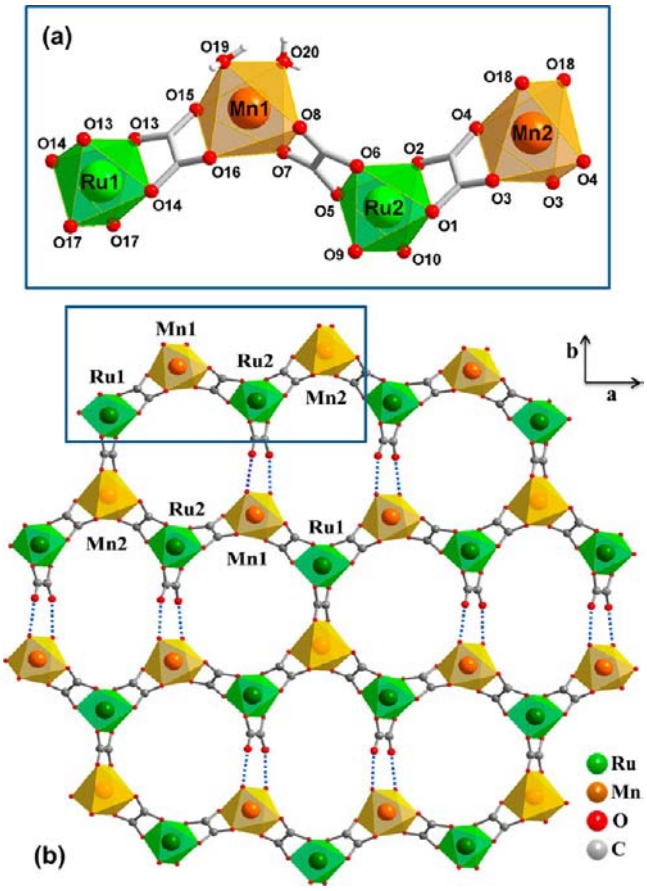

Figure 3. Representation of 2D honeycomb-like (6,3)-network, view along *c*-axis (b) and secondary building unit (a) (zigzag-like motif in applied zone) of compound **1**.

In the infrared spectra (see Figure S5) of compounds **1**–**5**, broad absorption bands at 1715–1713 and 1696–1679 cm^{-1} could be assigned to the symmetric and asymmetric contribution of chelated oxalate C═O bonds (ν_sC═O and ν_{as}C═O), respectively. Two other strong peaks at 1424–1412 cm^{-1} (ν_sC–O + ν_sC–C) and 1279–1264 cm^{-1} (ν_{as}C–O + ν_{as}C–C) are assigned to symmetric and asymmetric vibrations of oxalate C–O and C–C bonds. The absorption bands between 400 and 615 cm^{-1} show the presence of $\nu_{M\text{-}O}$ bonds, while absorptions at 825, 992, and 1106 cm^{-1} are due to C–C stretching vibrations.[20] The presence of coordinated water molecules is confirmed by the presence of a broad band in the region 3500–3200 cm^{-1}, which is due to O–H stretching vibrations. The incorporation of $[K(18\text{-crown-}6)]^+$ complex in the structures **1**–**5** is confirmed by the presence of bands between 2955 and 2920 cm^{-1}, which are associated with C–H stretching frequencies of the crown ring.[21]

Thermal stability in nitrogen and air atmosphere of compounds **1**–**5** was investigated. Thermal decomposition profiles, as shown in Figure S6, are similar for all title materials. For each compound the thermal analysis data are summarized in Table S1. Degradation process in nitrogen atmosphere of compound **1** has been taken as representative example. As shown in Figure S7, the thermal decomposition process proceeds in three stages. The first mass loss between 40 and 110 °C with the total mass loss of 1.5% (calcd 1.6%), corresponds to the gradual loss of the two water molecules coordinated to Mn1 atoms, which is accompanied by an

dx.doi.org/10.1021/ic302725v | *Inorg. Chem.* 2013, 52, 3933–3941

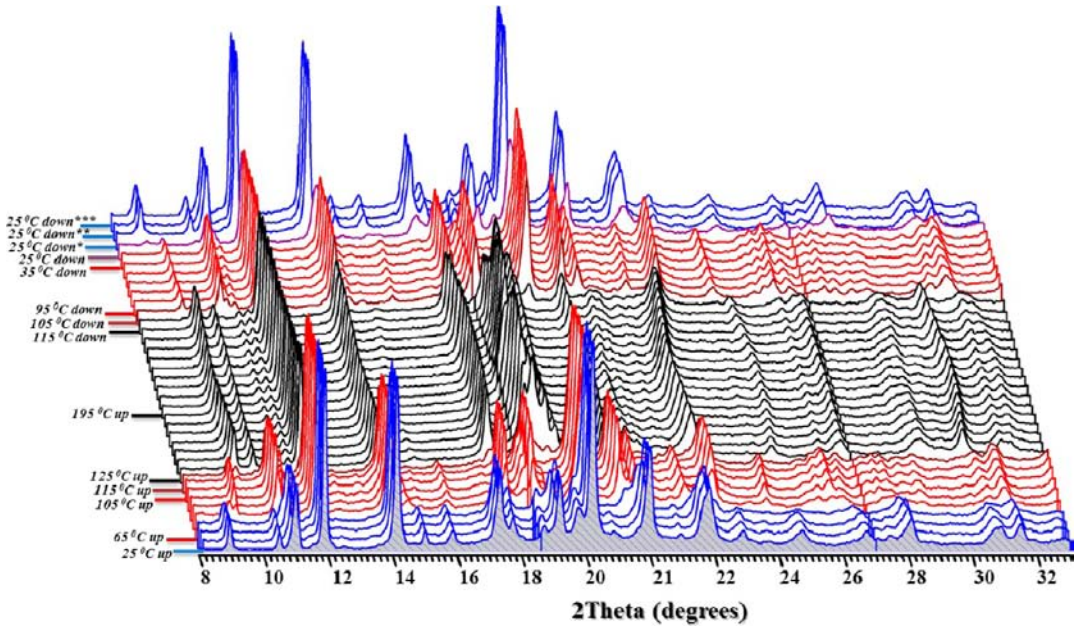

Figure 4. Powder X-ray thermodiffractograms of compound **1** recorded in air heating up from 25 to 195 °C and cooling down to 25 °C. Color code corresponding to the structural changes: blue, compound **1**; red, partially dehydrated compound **1a**; black, dehydrated compound **1b**. Asterisk marked pattern are recorded at 25 °C after half (*), one (**), and three (***) hour after experiment.

endothermic peak in the SDTA and DSC curves. The second step observed in the range 110−160 °C (endothermic process), with the total mass loss of 1.5% (calcd 1.6%), corresponds to loss of the last two water molecules coordinated to Mn1 atoms. These two steps of losing water molecules, confirmed by additional experiments in air atmosphere (see Figure S8), have been observed as endothermic peaks in the range 40−160 °C in SDTA and DSC curves. Up to 270 °C the compound remains stable until the third stage, which takes place in the range 270−350 °C (continuous process) with the total mass loss of *ca.* 64.3%, and corresponds to the progressive decomposition of the crown fragment and oxalate ligand, associated with endothermic and exothermic peaks in nitrogen and air atmospheres, respectively. The associated mass spectrometry m/z 18 (H_2O), and m/z 44 (CO_2) curves are in a good agreement with TG/DTG curves and show that the first and the second stages are purely attributed to water mass loss. In contrast, the third stage is accompanied with mass losses of m/z 18 (H_2O) and m/z 44 (CO_2) due to decomposition of crown and oxalate ligands. The residual solids resulting after total decomposition of compounds **1**−**5** were investigated by PXRD, which have been identified as mixture of Ru metal, K_2O, and MO in nitrogen atmosphere and as mixtures of RuO_2, K_2O, and M_2O_3 (**2**, **4**, and **5**), MO_2 (**1**), or MO (**3**) in the thermal oxidative degradation process in air atmosphere.

The powder X-ray thermodiffraction analysis carried out under air atmosphere by heating from 25 to 195 °C and cooling down to 25 °C was performed for **1** (see Figure 4) as a representative example of the series. The results confirm that compound **1** exhibits two phase transformation corresponding to two dehydration processes. This first one is produced by losing two water molecules coordinated to Mn1 atom, and the second one is due to the loss of last two bonded water molecules remaining in the partially dehydrated phase. Both partially and dehydrated phases exhibit a spontaneous rehydration processes after cooling down to room temperature (deep blue powder patterns at 25 °C down). For compound **1** no structural changes occur below 45 °C. The first phase transformation which leads to partially dehydrated compound **1a** begins at 55 °C, and the total transformation is reached at 75 °C and maintained until 105 °C, which is consistent with the TG analysis. The second phase transformation begins at 115 °C, and the total transformation to the anhydrous phase **1b** is reached at 125 °C and maintained until 195 °C. During the temperature decrease the anhydrous phase is preserved, and the first rehydration step begins at 95 °C and continues until room temperature giving the phase **1a**. In contrast, the second rehydration step is not achieved at the end of the experiment and requires a few additional hours in air, indicating the slow reversibility of this process compared with the previous one. It is worth mentioning that the peak at 2θ = ∼11° (at 25 °C), corresponding to interlayer distance in **1** (8.16 Å), is shifted to 10.6° (at 85 °C) and 10.3° (at 185 °C) due to increasing of interlayer spacing to *ca.* 8.4 Å and 8.6 Å for **1a** and **1b**, respectively. Powder X-ray diffraction patterns of partially dehydrated **1a** (at 65 °C) and anhydrous **1b** (at 185 °C) phases have been indexed in the monoclinic crystal system with the following unit cell dimensions: a = 19.33(1) Å, b = 11.46(1) Å, c = 14.46(1) Å, V = 3181.1(3) Å^3, for **1a**; a = 18.52(1) Å, b = 8.58(1) Å, c = 16.00(6) Å, V = 2543.7(2) Å^3, for **1b**. The results reveal that the unit cell contracts after dehydration processes maintaining the monoclinic crystal symmetry.

The catalytic activities of compounds **1**−**5** have been evaluated to behave as Lewis acid catalysts in the acetalyzation reaction of benzaldehyde with trimethylorthoformate (Scheme 1). In model experiments, the reaction was catalyzed in CCl_4 by using 1 mol % of catalyst affording phenyldimethylacetal in moderate to good yields: 49.8% for **1** (MnRu); 53.3% for **2** (FeRu); 85.2% for **3** (CoRu); 96.0% for **4** (CuRu); 82.6% for **5** (ZnRu) after 24 h at 70 °C (Figure 5). The TOF values (min^{-1}) obtained (124 (**1**); 133 (**2**); 213 (**3**); 240 (**4**); 206 (**5**)) indicate that the catalytic activity is higher than the reported previously for 2D and 3D coordination polymers.[22,23] In addition, the catalysts are easily separated from the resulting

dx.doi.org/10.1021/ic302725v | *Inorg. Chem.* 2013, 52, 3933−3941

Scheme 1. Acetalyzation of Benzaldehyde with Trimethyl Orthoformate

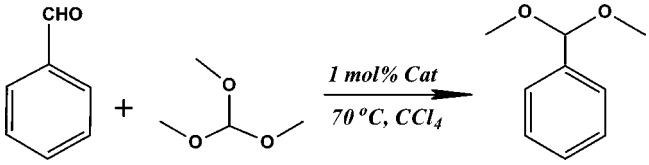

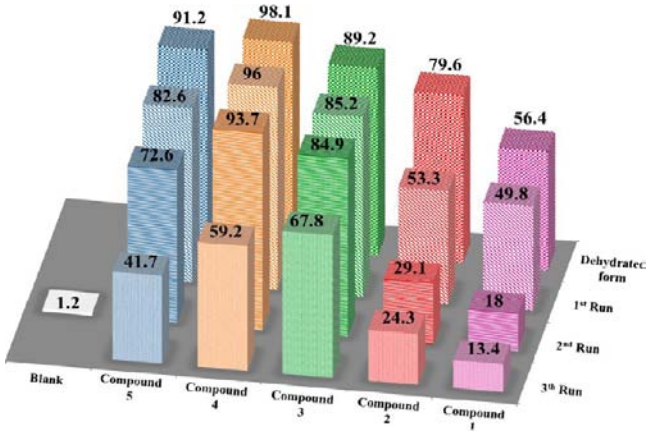

Figure 5. Catalytic properties of compounds **1**−**5** and their dehydrated forms **1b**−**5b** in reaction of benzaldehyde acetalyzation with TMOF at different catalytic runs. Reaction conditions: benzaldehyde (0.05 mL, 0.5 mmol), TMOF (0.5 mL, 5 mmol), CCl_4 (3 mL), heterogeneous catalyst (1 mol %), temperature 70 °C, under N_2 atmosphere. Conversion yields were determined by GC-FID. Blank run was carried out without heterogeneous catalyst.

solution by simple sedimentation (Figure S10). After the first catalytic run, catalysts **1**−**5** have been recovered by filtration, washed, and reused in two further consecutive runs. As expected, the resulting yields decrease (2nd run, 18 − 93.7%; third run, 13.4 − 41.7%) due to the partial mass loss of the catalyst. For comparison, a blank experiment without catalyst was carried out under the same reaction conditions obtaining a thermal conversion of only 1.2%. In addition, it is interesting to mention that when the catalyst **1** is removed by centrifugation after 5 h of reaction (23%), no significant transformation is observed (see Figure S9). This indicates that the catalytic activity is originated by active sites of the heterogeneous catalyst, rather than the molecular species contained in the filtrate which can be generated from the leaching of the solid catalyst. Also, after three catalytic runs catalyst **1** has been isolated and characterized by PXRD proving its thermal stability (Figure S11). As it was indicated above, coordinated water molecules in compounds **1**−**5** can be easily removed by heating under vacuum generating free coordination sites at the metal M^{II} center. In order to test the catalytic activity of the dehydrated solids, compounds **1**−**5** were totally dehydrated before their use as catalysts. Under the same reaction conditions, i.e., 1 mol % of catalyst loading, using CCl_4 as a solvent, and heating at 70 °C during 24 h, the phenyldimethylacetal is obtained in higher yields (56.4% vs 49.8% (**1**); 79.6% vs 53.3% (**2**); 89.2% vs 85.2% (**3**); 98.1% vs 96% (**4**); 91.2% vs 82.6% (**5**)), as compared with those obtained using hydrated forms (Figure 5). It is obvious that the dehydration gives rise to Lewis acid centers with an enhanced strength toward benzaldehyde and hence improved catalytic performance. The generation of Lewis acid centers in metal−organic frameworks $[Cu_3(BTC)_2(H_2O)_3]\cdot xH_2O$ (BTC = benzene 1,3,5-tricarboxylate) by removal of the copper(II) bonded water molecules is also known.[22] The higher catalytic activity observed for the dehydrated MOF $[Cu_3(BTC)_2]$ is reasoned on the basis of the easier access to the copper(II) sites. It is worth mentioning that the catalytic activity for hydrated and anhydrous compounds **1**−**5** follows the sequence **1** < **2** < **3** < **4** > **5** in a similar way as the Irving−Williams series for the formation constants of divalent metal ions $Mn^{2+} < Fe^{2+} < Co^{2+} < Ni^{2+} < Cu^{2+} > Zn^{2+}$. As it is well-known, this sequence results from the decrease of the ionic radii as well as the ligand field stabilization energies.[24] The exceptional Cu(II) position, in spite of its d^9 electronic configuration, arises from the additional stabilization energy due to the Jahn−Teller distortion which leads to a tetragonal distorted coordination environment. The highest catalytic activity shown by compound **4** is probably reflecting the enhanced binding energy of benzaldehyde which is coordinated in the equatorial plane and therefore is undergoing the strongest Lewis acid interaction. Finally, it is worth noting that a much lower catalytic performance is found when the salt $Cu(NO_3)_2\cdot 4H_2O$ is used as catalyst (1.8% yield of diphenylmethylacetal after heating in CCl_4 for 24 h) which means that the Lewis acid sites incorporated into the coordination polymers play a key catalytic role. In summary, these results show further examples of the utility of 2D coordination polymers as efficient heterogeneous catalysts which also can be easily recovered by filtration and reused in three cycles.

Variable temperature magnetic susceptibility measurements of compound **1**−**5** have been carried out on powdered samples in the 2−250 K temperature range. The temperature dependence of the molar magnetic susceptibilities, χ_m, and the reciprocal, χ_m^{-1}, is represented in Figure 6. The linear

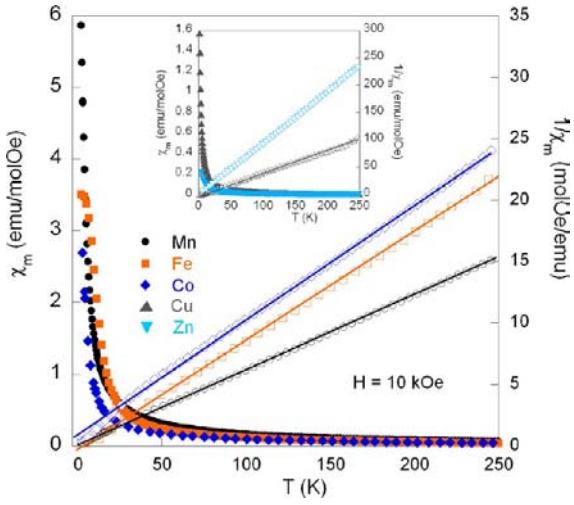

Figure 6. Temperature dependence of molar magnetic susceptibilities, χ_m, and reciprocal, χ_m^{-1}, for compounds **1**−**3** (M^{II} = Mn (**1**), Fe (**2**), Co (**3**)). The inset shows the variations corresponding to the compounds **4** and **5** (M^{II} = Cu (**4**), Zn (**5**)).

behavior of χ_m^{-1} at high temperatures can be fitted to a Curie−Weiss law for all investigated compounds. The experimental and calculated values of the effective paramagnetic moments and the paramagnetic Curie temperatures are gathered in Table 2. The values of the paramagnetic Curie−Weiss temperatures, θ, do not show any clear trend, with positive and negative

dx.doi.org/10.1021/ic302725v | Inorg. Chem. 2013, 52, 3933−3941

Table 2. Main Magnetic Data for Compounds 1−5 (M^{II} = Mn (1), Fe (2), Co (3), Cu (4), and Zn (5))[a]

compd/ M^{II}	μ_{eff} (μ_B/molecule)	μ_{eff} (μ_B/M^{II})	μ^{teo}_{eff} (μ_B/M^{II})	θ (K)	M (μ_B/molecule), T = 2K, H = 85 kOe
1/Mn	11.43(1)	6.37	5.90	−0.91(1)	16.05(1)
2/Fe	9.40(1)	5.16	5.40	6.84(1)	8.81(1)
3/Co	9.16(1)	5.01	4.80	−3.73(1)	7.76(1)
4/Cu	4.42(1)	1.92	1.90	1.33(1)	4.98(1)
5/Zn	2.91(1)	0.00	0.00	2.16(1)	2.72(1)

[a]Paramagnetic moments (for the molecule, for the M^{2+} magnetic moments and the theoretical expected ones) extracted from the high temperature behavior of the magnetic susceptibility, paramagnetic Curie temperature, and maximum magnetic moment measured under 85 kOe at 2 K (see text).

values, such that $|\theta| < 7$ K. This feature indicates that these compounds are characterized by the existence of competing magnetic interactions, which are too weak (except for those of the compound **2**, the Fe-based one) to establish magnetic ordering. This situation is not surprising because, in other related Ru^{III}-transition metal systems mediated through the oxalate bridge, ferromagnetic[14a] or antiferromagnetic[14b] states have been reported. The fact that compound **5** has a totally filled 3d shell means that the paramagnetic value of 2.91 μ_B could be associated with the paramagnetic moment of the Ru^{3+} ions. Taking into account this, the values of the paramagnetic moments of **1**−**4** can be extracted (see Table 2). The comparison of the experimental paramagnetic moments with the theoretical expected values obtained from the quenching of the orbital magnetic moment is in good agreement (see Table 2). No magnetic ordering has been detected in all the investigated compounds, except for the compound **2**, where the results of the magnetization at different magnetic fields, measured warming under a certain magnetic field after cooling down at zero field from room temperature first, without applied magnetic field (ZFC) and subsequently under applied magnetic field (FC), are shown in Figure 7. The low-temperature behavior is characterized by a sharp maximum in the ZFC-FC

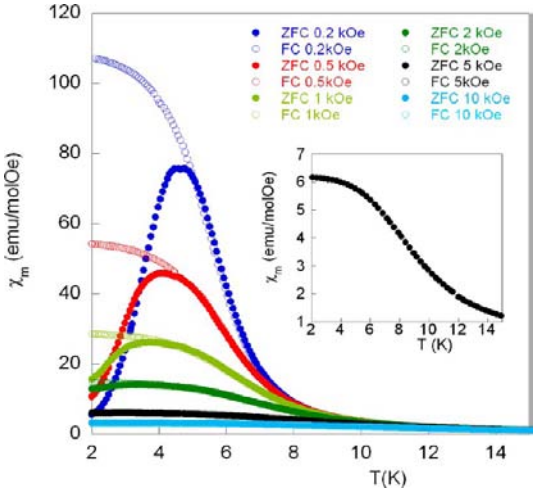

Figure 7. Low-temperature dependence of molar magnetic susceptibility, χ_m, for compound **2** (M^{II} = Fe), under ZFC and FC conditions. The inset shows the detail of the low-temperature behavior of χ_m under 10 kOe.

signals at temperature near T_f = 5 K under 0.2 kOe that shifts to low temperature as the intensity of the applied magnetic field increases, and disappearing under 5 kOe, where no maximum and irreversibility is observed in the ZFC-FC measurements (see inset of Figure 7). This effect of irreversibility observed in the magnetization curves is characteristic of a spin-glass-like behavior, which is suppressed using low magnetic fields. Magnetization data for all the investigated compounds have been measured as a function of field at 2 K under magnetic fields up to 85 kOe (Figure 8). The saturation magnetization

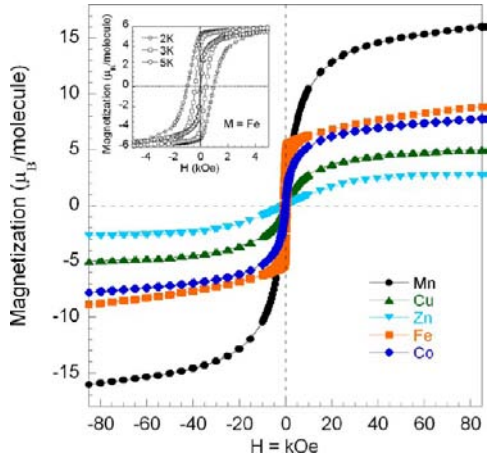

Figure 8. Magnetic hysteresis loops, $M(H)$, for **1**−**5** (M^{II} = Mn (**1**), Fe (**2**), Co (**3**), Cu (**4**), Zn (**5**)) collected at 2 K. The inset shows the detail of the loops around H = 0 for the investigated temperatures below T_f = 5 K for compound **2** (M^{II} = Fe).

values at 2 K are gathered in Table 2. These values are smaller than the theoretical saturation magnetization moments for the transition M^{II} metals. All of them have neither coercivity or remanence, except the case of compound **2** (M^{II} = Fe), where the coercive field reaches a value close to 1 kOe at 2 K. For this last compound magnetization has been also measured at 3, 4, and 5 K. Whereas the saturation magnetization is nearly constant, the coercive field decreases from 930 to 640, 410 Oe for 3 and 4 K, respectively, disappearing for 5 K, in good agreement with magnetic susceptibility data.

In order to study a possible dynamical response in compound **2**, ac measurements were carried out with an alternating excitation field of 3 Oe at different frequencies from 0.01 to 10^3 Hz. The real (M') and out-of phase (M'') components of the susceptibility are shown in Figure 9. In a first view, the existence of a sharp peak around 5 K in both M' and M'' parts could be indicative of the possible presence of a spin-glass state. The M' values present a slight shift with the frequency whereas the peak height is almost constant. The more significant feature is that the position of the maximum shifts to higher temperatures with increasing frequency, which is usually considered as fingerprint of the spin-glass transition.[25] The freezing temperature T_f, associated with the spin-glass state, corresponds to the maximum in real part, M'. Depending on the interactions between the magnetic moments, T_f can be weakly (strong interactions) or strongly (weak interactions) dependent on the frequency (see Figure 9). In compound **2**, the frequency shifts the freezing temperature, within experimental errors, 0.015 (see inset of Figure 9a). Following Mydosh analysis,[26] the frequency dependence of the maximum agrees with the empirical Vogel−Fulcher law

dx.doi.org/10.1021/ic302725v | Inorg. Chem. 2013, 52, 3933−3941

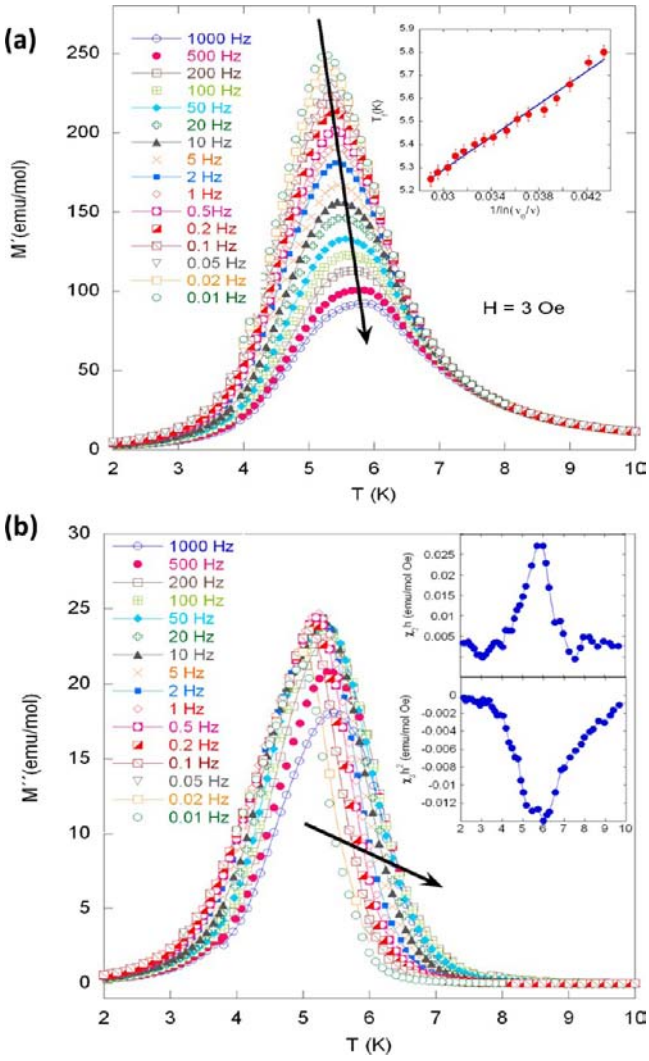

Figure 9. In-phase (M′) and out-of-phase (M″) ac magnetization for compound **2** (M^{II} = Fe) measured under different excitation frequencies from 1000 to 0.01 Hz. The inset on part b shows the temperature variations of the nonlinear susceptibilities χ_2 and χ_3, when the static applied magnetic field H = 0, and the alternating excitation field h = 3 Oe, and the frequency = 1 kHz.

$$\tau_m = \tau_o \exp\left[\frac{E_a}{k_B(T_f - T_o)}\right]$$

with the relaxation time τ_o characteristic of strong interactions and weak frequency dependence of the freezing temperature. Assuming the variation of M′ to a Gaussian function around T_f and taking $\nu_o = \tau_o^{-1} = 10^{13}$ Hz,[27] we obtain reasonable fitting parameters of the activation energy E_a and the Vogel–Fulcher temperature T_o with E_a = 35.5 K and T_o = 4.2 K. These values are similar to those observed for other iron insulator spin-glasses previously reported.[28]

A combined investigation of both odd and even harmonics of the ac magnetic response enables one to distinguish between a canonical and a cluster spin glass.[29] While the odd harmonics yield true asymptotic values of the critical exponents of the spin glasses, the even harmonics can confirm the presence or absence of correlated spin regions (spin clusters). In this sense, the even harmonics of the nonlinear susceptibilities χ_2 and χ_4 are zero[30] for an ideal SG at temperatures $T \sim T_f$. By contrast, for a ferromagnet, χ_2 and χ_4 are finite.[31] On the basis of these considerations, the $\chi_2(T)$ and $\chi_3(T)$ data, presented in the inset of Figure 9, provide direct evidence for the existence of two different time (and hence length) scales for the SG and FM order in compound **2**. A global SG order and a small contribution of short-range FM order (it is likely due to the existence of cluster Fe rich domains) are observed at the experimental time scales.

CONCLUSIONS

A series of isostructural coordination polymers based on a ruthenium trioxalate building unit and several transition metals $\{[K(18\text{-crown-}6)]_3[M^{II}_3(H_2O)_4\{Ru(ox)_3\}_3]\}_n$ (M^{II} = Mn (**1**), Fe (**2**), Co (**3**), Cu (**4**), Zn (**5**)) have been synthetized and structurally characterized. Topological simplification of isostructural 2D frameworks gives rise to a uninodal three-connected net with hcb hexagonal plane type. This series of compounds have been obtained as a microcrystalline powders and exhibit high thermal stability. Also, the compounds **1**–**5** exhibit two phase transformations characterized by spontaneous rehydration processes with different kinetics. All the coordination polymers **1**–**5** behave as highly active Lewis acid catalysts in the acetalyzation reaction of benzaldehyde with trimethylorthoformate exhibiting an increased activity in the sequence $Mn^{2+} < Fe^{2+} < Co^{2+} < Ni^{2+} < Cu^{2+} > Zn^{2+}$, and can be reused in three consecutive runs preserving a considerable catalytic activities. The dehydrated coordination polymers **1b**–**5b** show higher catalytic performances due to the creation of active-accessible Lewis acid centers. The magnetic susceptibility shows that all the investigated compounds do not present any long-range magnetic order down to 2 K. The Fe-based compound **2** shows the existence of a cluster spin-glass-like state below 5 K, characterized by the presence of a magnetic irreversibility in the ZFC-FC magnetization data. Alternating current magnetic susceptibility shows the presence of a maximum at 5 K that shifts to higher temperatures with increasing frequency. The coercive field increases as the temperature is lowered below 5 K, reaching a value of 1 kOe at 2 K.

ASSOCIATED CONTENT

Supporting Information

SEM images, IR spectra, thermoanalytical data, and X-ray crystallographic information (CIF data) for compounds **1**–**5**. This material is available free of charge via the Internet at http://pubs.acs.org.

AUTHOR INFORMATION

Corresponding Author

*E-mail: jrgm@uniovi.es.

Notes

The authors declare no competing financial interest.

ACKNOWLEDGMENTS

The authors thank FEDER and Spanish MINECO for financial support under projects MAT2010-15094, MAT2008-06542-C04-03, MAT2011-27573-C04-02, and FC-08-IB08-036. A.D. also thanks the Spanish Ministerio de Educación, Cultura y Deporte for the predoctoral FPU grant (AP2008-03942).

REFERENCES

(1) (a) Batten, S. R.; Neville, S. M.; Turner, D. R. *Coordination Polymers. Design, Analysis and Applications*; RSC Publishing Cambridge: Cambridge, U.K., 2009. (b) Long, J. R.; Yaghi, O. M. *Chem. Soc. Rev.* **2009**, *38*, 1213−1214. (c) Zhou, H.-C.; Long, J. R.; Yaghi, O. M. *Chem. Rev.* **2012**, *112*, 673−674.

(2) (a) Corma, A.; García, H.; Llabrés-Xamena, F. X. *Chem. Rev.* **2010**, *110*, 4606−4655. (b) Yoon, M.; Srirambalaji, R.; Kim, K. *Chem. Rev.* **2012**, *112*, 1196−1231. (c) Ma, L.; Abney, C.; Lin, W. *Chem. Soc. Rev.* **2009**, *38*, 1248−1256. (d) Lee, J. Y.; Farha, O. K.; Roberts, J.; Scheidt, K. A.; Nguyen, S.-B. T.; Hupp, J. T. *Chem. Soc. Rev.* **2009**, *38*, 1450−1459. (e) Farrusseng, D.; Aguado, S.; Pinel, C. *Angew. Chem., Int. Ed.* **2009**, *48*, 7502−7513.

(3) Fei, H.; Rogow, D. L.; Oliver, S. R. J. *J. Am. Chem. Soc.* **2010**, *132*, 7202−7209.

(4) (a) Suh, M. P.; Park, H. J.; Prasad, T. K.; Lim, D.-W. *Chem. Rev.* **2012**, *112*, 782−835. (b) Murray, L. J.; Dincă, M.; Long, J. R. *Chem. Soc. Rev.* **2009**, *38*, 1294−1314. (c) Li, J.-R.; Kuppler, R. J.; Zhou, H.-C. *Chem. Soc. Rev.* **2009**, *38*, 1477−1504. (d) Sumida, K.; Rogow, D. L.; Mason, J. A.; McDonald, T. M.; Bloch, E. D.; Herm, Z. R.; Bae, T.-H.; Long, J. R. *Chem. Rev.* **2012**, *112*, 724−781.

(5) (a) Cui, Y.; Yue, Y.; Qian, G.; Chen, B. *Chem. Rev.* **2012**, *112*, 1126−1162. (b) Kreno, L. E.; Leong, K.; Farha, O. K.; Allendorf, M.; Van Duyne, R. P.; Hupp, J. T. *Chem. Rev.* **2012**, *112*, 1105−1125. (c) Allendorf, M. D.; Bauer, C. A.; Bhakta, R. K.; Houk, R. J. T. *Chem. Soc. Rev.* **2009**, *38*, 1330−1352.

(6) (a) Kurmoo, M. *Chem. Soc. Rev.* **2009**, *38*, 1353−1379. (b) Zhang, W.; Xiong, R.-G. *Chem. Rev.* **2012**, *112*, 1163−1195.

(7) (a) Liang, L.; Peng, G.; Ma, L.; Sun, L.; Deng, H.; Li, H.; Li, W. *Cryst. Growth Des.* **2012**, *12*, 1151−1158. (b) Feng, R.; Chen, L.; Chen, Q.-H.; Shan, X.-C.; Gai, Y.-L.; Jiang, F.-L.; Hong, M.-C. *Cryst. Growth Des.* **2011**, *11*, 1705−1712. (c) Zhao, X.-Q.; Zhao, B.; Wei, S.; Cheng, P. *Inorg. Chem.* **2009**, *48*, 11048−11057.

(8) (a) Su, Z.; Fan, J.; Okamura, T.-A.; Sun, W.-Y.; Ueyama, N. *Cryst. Growth Des.* **2010**, *10*, 3515−3521. (b) Li, L.; Niu, S.-Y.; Jin, J.; Meng, Q.; Chi, Y.-X.; Xing, Y.-H.; Zhang, G.-N. *J. Solid State Chem.* **2011**, *184*, 1279−1285. (c) Sun, D.; Wang, D.-F.; Han, X.-G.; Zhang, N.; Huang, R.-B.; Zhenga, L.-S. *Chem. Commun.* **2011**, *47*, 746−748.

(9) (a) Coronado, E.; Galán-Mascarós, J. R.; Martí-Gastaldo, C. *J. Mater. Chem.* **2006**, *16*, 2685−2689. (b) Mathonière, C.; Nuttall, K. J.; Carling, S. G.; Day, P. *Inorg. Chem.* **1996**, *35*, 1201−1206. (c) Tamaki, H.; Zhong, Z. J.; Matsumoto, N.; Kida, S.; Koikawa, M.; Achiwa, N.; Hashimoto, Y.; Okawa, H. *J. Am. Chem. Soc.* **1992**, *114*, 6974−6979. (d) Min, K. S.; Rhinegold, A. L.; Miller, J. S. *Inorg. Chem.* **2005**, *44*, 8433−8441. (e) Ovenesyan, N. S.; Makhaev, V. D.; Aldoshin, S. M.; Gredin, P.; Boubekeur, K.; Train, C.; Gruselle, M. *Dalton Trans.* **2005**, 3101−3107. (f) Decurtins, S.; Schmalle, H. W.; Osward, H. R.; Linden, A.; Ensling, J.; Gütlich, P.; Hauser, A. *Inorg. Chim. Acta* **1994**, *216*, 65−73.

(10) (a) Coronado, E.; Galán-Mascarós, J. R.; Martí-Gastaldo, C.; Waerenborgh, J. C.; Gaczyński, P. *Inorg. Chem.* **2008**, *47*, 6829−6839. (b) Coronado, E.; Galán-Mascarós, J. R.; Martí-Gastaldo, C. *Inorg. Chem.* **2006**, *45*, 1882−1884. (c) Andrés, R.; Gruselle, M.; Malézieux, B.; Verdaguer, M.; Vaissermann, J. *Inorg. Chem.* **1999**, *38*, 4637−4646. (d) Coronado, E.; Galán-Mascarós, J. R.; Martí-Gastaldo, C. *J. Am. Chem. Soc.* **2010**, *132*, 5456−5468. (e) Coronado, E.; Galán-Mascarós, J. R.; Martí-Gastaldo, C. *J. Am. Chem. Soc.* **2008**, *130*, 14987−14989. (f) Coronado, E.; Galán-Mascarós, J. R.; Gómez-García, C. J.; Martí-Gastaldo, C. *Inorg. Chem.* **2005**, *44*, 6197−6202. (g) Coronado, E.; Galán-Mascarós, J. R.; Martí-Gastaldo, C. *Inorg. Chem.* **2007**, *46*, 8108−8110. (h) Coronado, E.; Galán-Mascarós, J. R.; Martí-Gastaldo, C. *Inorg. Chim. Acta* **2008**, *361*, 4017−4023. (i) Coronado, E.; Galán-Mascarós, J. R.; Martí-Gastaldo, C. *Polyhedron* **2007**, *26*, 2101−2104.

(11) (a) Rao, C. N. R.; Natarajan, S.; Vaidhyanathan, R. *Angew. Chem., Int. Ed.* **2004**, *43*, 1466−1496. (b) Coronado, E.; Clemente-León, M.; Galán-Mascarós, J. R.; Giménez-Saiz, C.; Gómez-García, C. J.; Martínez-Ferrero, E. *J. Chem. Soc., Dalton Trans.* **2000**, 3955−3961. (c) Cheetham, A. K.; Rao, C. N. R.; Feller, R. K. *Chem. Commun.* **2006**, 4780−4795.

(12) Coronado, E.; Galán-Mascarós, J. R.; Gómez-García, C. J.; Laukhin, V. *Nature* **2000**, *408*, 447−449.

(13) (a) McClaverty, J. A.; Mayer, T. J. *Comprehensive Coordination Chemistry II. From Biology to Nanotechnology. Transition Metal Groups 7 and 8*; Elsevier Ltd.: Oxford, U.K., 2004; Vol. 5. (b) Seddon, E. A.; Seddon, K. R. *Ruthenium Chemistry*; Elsevier Science Publishers B. V.: Amsterdam, The Netherlands, 1984.

(14) (a) Coronado, E.; Galán-Mascarós, J. R.; Gómez-García, C. J.; Martínez-Agudo, J. M.; Martínez-Ferrero, E.; Waerenborgh, J. C.; Almeida, M. *J. Solid State Chem.* **2001**, *159*, 391−402. (b) Larionova, J.; Mombelli, B.; Sanchiz, J.; Kahn, O. *Inorg. Chem.* **1998**, *37*, 679−684.

(15) (a) Murahashi, S.-I. *Ruthenium in Organic Synthesis*; Wiley-VCH: New York, 2004. (b) Bruneau, C.; Dixneuf, P. H. *Ruthenium Catalysts and Fine Chemistry (Topics in Organometallic Chemistry)*; Springer-Verlag: New York, 2004.

(16) Kaziro, R.; Hambley, T. W.; Bistead, R. A.; Beattie, J. K. *Inorg. Chim. Acta* **1989**, *164*, 85−91.

(17) http://accelrys.com/products/materials-studio/

(18) Boultif, A.; Louer, D. *J. Appl. Crystallogr.* **2004**, *37*, 724−731.

(19) Blatov, V. A.; Shevchenko, A. P. *TOPOS-Version 4.0 Professional (beta evaluation)*; Samara State University: Samara, Russia, 2006.

(20) Nakamoto, K. *Infrared and Raman Spectra of Inorganic and Coordination Compounds, Part B.*; John Wiley & Sons Inc.: New York, 2009.

(21) Socrates, G. *Infrared and Raman Characteristic Group Frequencies*; John Wiley & Sons Ltd: London, U.K., 2001.

(22) (a) Amghouz, Z.; Roces, L.; García-Granda, S.; García, J. R.; Souhail, B.; Mafra, L.; Shi, F.; Rocha, J. *Inorg. Chem.* **2010**, *49*, 7917−7926. (b) Amghouz, Z.; García-Granda, S.; García, J. R.; Ferreira, R. A. S.; Mafra, L.; Carlos, L. D.; Rocha, J. *Inorg. Chem.* **2012**, *51*, 1703−1716. (c) Gándara, F.; Gomez-Lor, B.; Gutiérrez-Puebla, E.; Iglesias, M.; Monge, M. A.; Proserpio, D. M.; Snejko, N. *Chem. Mater.* **2008**, *20*, 72−76. (d) Perles, J.; Iglesias, M.; Ruiz-Valero, C.; Snejko, N. *Chem. Commun.* **2003**, 346−347. (e) Bernini, M. C.; Gándara, F.; Iglesias, M.; Snejko, N.; Gutiérrez-Puebla, E.; Brusau, E. V.; Narda, G. E.; Ángeles Monge, M. *Chem.—Eur. J.* **2009**, *15*, 4896−4905. (f) Gomez-Lor, B.; Gutiérrez-Puebla, E.; Iglesias, M.; Monge, M. A.; Ruiz-Valero, C.; Snejko, N. *Inorg. Chem.* **2002**, *41*, 2429−2432. (g) Perles, J.; Iglesias, M.; Ruiz-Valero, C.; Snejko, N. *J. Mater. Chem.* **2004**, *14*, 2683−2689. (h) Gómez-Lor, B.; Gutiérrez-Puebla, E.; Iglesias, M.; Monge, M. A.; Ruiz-Valero, C.; Snejko, N. *Chem. Mater.* **2005**, *17*, 2568−2573.

(23) (a) Schlichte, K.; Kratzke, T.; Kaskel, S. *Microporous Mesoporous Mater.* **2004**, *73*, 81−88. (b) Dhakshinamoorthy, A.; Álvaro, M.; García, H. *Adv. Synth. Catal.* **2010**, *352*, 3022−3030. (c) Alaerts, L.; Séguin, E.; Poelman, H.; Thibault-Starzyk, F.; Jacobs, P. A.; De Vos, D. E. *Chem.—Eur. J.* **2006**, *12*, 7353−7363.

(24) Schriver, D.; Atkins, P. W. *Inorganic Chemistry*, 5th ed.; Oxford University Press: Oxford, U.K., 2010.

(25) Fischer, K. H.; Hertz, J. *Spin Glasses*; Cambridge University Press: Cambridge, U.K., 1991.

(26) Mydosh, J. A. *Spin Glasses: An Experimental Introduction*; Taylor & Francis: London, U.K., 1993.

(27) Tholence, J. L. *Solid State Commun.* **1980**, *35*, 113−117.

(28) Chan Chung, U.; Mesa, J. L.; Pizarro, J. L.; Meatza, I.; Bengoechea, M.; Rodríguez Fernández, J.; Arriortua, M. I.; Rojo, T. *Chem. Mater.* **2011**, *23*, 4317−4330.

(29) Bitla, Y.; Kaul, S. N.; Fernández-Barquín, L. *Phys. Rev. B* **2012**, *86*, 094405(1)−(9).

(30) (a) Suzuki, M. *Prog. Theor. Phys.* **1977**, *58*, 1151−1165. (b) Wada, K.; Takayama, H. *Prog. Theor. Phys.* **1980**, *64*, 327−329. (c) Fujiki, S.; Katsura, S. *Prog. Theor. Phys.* **1981**, *65*, 1130−1144.

(31) Bitla, Y.; Kaul, S. N. *Europhys. Lett.* **2011**, *96*, 37012(1)−(6).